The Effect of Carbon Nanotube Composite Addition on Biomass-Based Supercapacitor

Pramujo Widiatmoko, Hary Devianto*, Isdiriayani Nurdin & Ridho Eko Yandra

Department of Chemical Engineering, Faculty of Industrial Technology,
Institut Teknologi Bandung, Jalan Ganesa No. 10, Bandung 40132, Indonesia
*E-mail: hardev@che.itb.ac.id

Abstract. Electric vehicles are set to become a most attractive alternative transportation mode due to their high efficiency and low emission. Electric vehicles require an efficient energy storage system, e.g. a supercapacitor. Coconut shells have high lignocellulosic content and are not being fully utilized in Indonesia. The lignocellulose could be converted into activated carbon for use as the electrode on a hybrid supercapacitor. This research focused on studying the effect of the addition of carbon nanotube (CNT) composite to porous graphene-like nanosheets (PGNS) as the electrode on a hybrid supercapacitor. The PGNS and CNT composite were synthesized via simultaneous activation and carbonization. Nickel oxide was used as the counter electrode. The CNT composite had a large surface area of 1374.8 m^2g^{-1}, pore volume of 1.1 cm^3g, and pore size of 3.2 nm. On the other hand, the PGNS had a surface area of 666.1 m^2g^{-1}, pore volume of 0.47 cm^3g , and pore size of 2.8 nm. The electrode pair between the NiO and the activated carbon achieved 5.69 F/g and 94.1% cycle durability after 10 charging and discharging cycles. The composite had an energy density of 0.38 W h kg^{-1}. The aim of this research was to provide an alternative formula for producing high-performance supercapacitor materials.

Keywords: *coconut shell; carbon nanotube; energy storage; hybrid supercapacitor porous graphene.*

1 Introduction

The *Annual Energy Outlook 2014* published by the U.S. Energy Information Administration, which is focused on a projection of macroeconomic, residential, commercial, and industrial energy consumption, reports that more than 80% of the world's total energy needs are supplied by fossil fuels [1]. With the depletion of the fossil fuel reserve and increasing concern about pollution due to greenhouse gases, the development of alternative energy sources is imperative. Electricity is assumed to be the best form of energy due to its high-energy conversion efficiency.

Rapid development of electric vehicle technology requires high-performance electrical energy storage. Batteries, as well known electrical energy storage devices, suffer from a short life cycle. Meanwhile, conventional capacitors

Received May10th, 2016, Revised October 20th, 2016, Accepted for publication November 17th, 2016.
 ISSN: 2337-5779, DOI: 10.5614/j.eng.technol.sci.2016.48.5.7

retain low capacitance despite their fast discharge capability. To overcome these issues, the supercapacitor has been developed [2]. Supercapacitors provide higher capacitance than conventional capacitors (in the Farad range), while having a longer life cycle than batteries.

Activated carbon from biomass can potentially be applied to the supercapacitor's electrode due to its large surface area, well-distributed nanopore volume and size, high availability and low price [3]. Indonesia has a huge biomass resource in the form of coconut shells from its 3.86 million hectares of coconut plantations (31.2% of the total area in the world), producing 15 billion coconuts annually [4]. However, there has been limited research into the utilization of coconut shells for supercapacitor application.

There are two categories of supercapacitors differentiated by the charge storage mechanism: electrical double layer capacitors (EDLC) and pseudocapacitors. Hybrid supercapacitors combine the advantages of the EDLC and the pseudocapacitor, i.e. high power and energy density. In this research, we prepared a hybrid supercapacitor from activated carbon (as EDLC electrode) and metal oxide (as pseudocapacitor electrode). The focus of this research was to study the effects of CNT addition to PGNS on the performance of the hybrid supercapacitor.

2 Methodology

It was expected that the composite composition of the carbon is the most influencing factor on the performance of the supercapacitor. This research consisted of the main steps as shown in Figure 1.

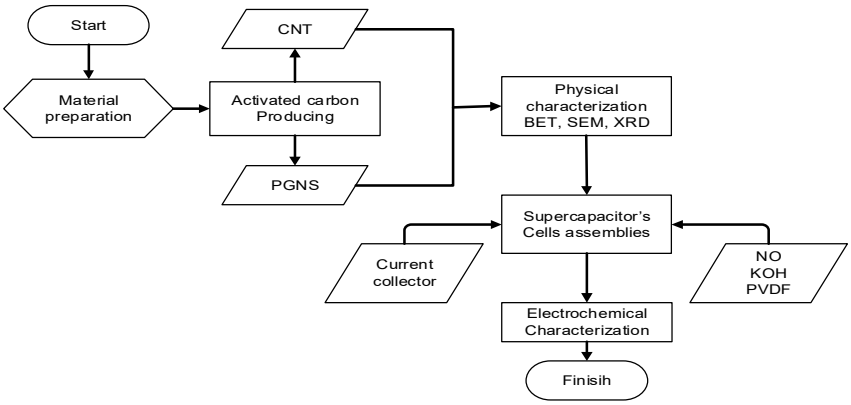

Figure 1 Research flow chart.

The prepared coconut shells as raw material were synthesized in two structural types of carbon, i.e. PGNS and CNT composite. Coconut shells were cleaned from dirt and then dried and pulverized into 200-400 mesh size. The pulverized coconut shells were mixed with $ZnCl_2$ and $FeCl_3$ and dried at 110 °C. The CNT was produced by inserting the mixture of coconut shell powder with $ZnCl_2$ and $FeCl_3$ into a stainless steel tube. The tube was welded shut at both tips and heated in a furnace at 900 °C for 1 h. To produce the PGNS, the procedure was the same, excluding the insertion of the mixture into a stainless steel tube. The mixture of coconut shell, $ZnCl_2$ and $FeCl_3$ was collected in a ceramic crucible and heated in a furnace at 900 °C for 1 h. Each synthesized activated carbon was then characterized by BET, SEM, and XRD. BET analysis was used to calculate the surface area, size distribution, and pore volume of the activated carbon. Determining the surface morphology of the activated carbon utilizing SEM analysis and XRD was used to identify the crystal structure of the activated carbon. The variations of activated carbon electrode composition are shown in Table 1.

Table 1 Variations of activated carbon electrode composition.

Variation	PGNS (%-wt)	CNT (%-wt)
1	100	0
2	90	10
3	80	20
4	70	30
5	60	40

NiO was used as the counter electrode after synthesis through simultaneous oxidation at 500 °C and Nafion 212 as a separator and KOH electrolyte. Electrochemical characterization was done by CV and EIS analysis. CV was used to calculate the resulted capacitance of each cell in a voltage range of 0-0.7 V, cycle ability until 10 cycles, and cell durability at a scan rate varied from 2-50 mV/s. The purpose of EIS is to observe the cell durability and conduct capacitance testing after being given disturbance. EIS was measured after the 1^{st} and the 10^{th} cycle in a frequency range of 10.000-0.01 Hz. The electrochemical testing scheme is shown in Figure 2.

The supercapacitor cell was connected electrically to the electrochemical testing equipment, a potensiostat Gamry V3000. In Figure 2, WE refers to the working electrode and CE refers to the counter electrode.

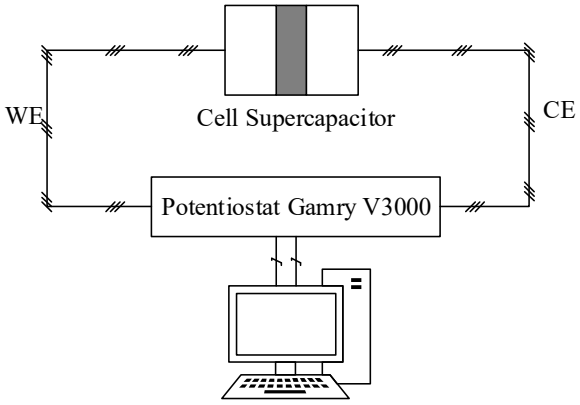

Figure 2 Supercapacitor electrochemical testing equipment scheme.

3 Result and Discussion

3.1 Modification Activated Carbon

Ideal supercapacitor performance depends on a combination of surface area and electrode conductivity. In this research, simple modifications of PGNS and CNT composite of coconut shell through simultaneous carbonization and activation were performed. A comparison between these two types of activated carbon modification is shown in Table 2.

Table 2 Comparative characteristics of activated carbon modifications.

Material	Size (mesh)	Temperature (°C)	S_{BET} (m^2g)	Average volume (cm^3g)	Average pore size (nm)
Coconut shell	200-400	-	2.9	0.008	11
PGNS	200-400	900	666.01	0.4	2.8
CNT composite	200-400	900	1374.8	1.1	3.2
Commercial carbon	Powder	-	501.4	0.2	2.3

As can be seen in Table 2, the modification of the activated carbon went well in the carbonization and coconut shell activation process. The temperature of 900 °C and the combination of activators $ZnCl_2$ and $FeCl_3$ were enough to decompose the coconut shell substrate so that the surface area of the sample could increase significantly. The pore size decreased along with the decomposition of non-carbon materials such as O_2, H_2, N_2 and tar, which covered the surface. The decomposition of non-carbon materials produces a volatile gas and leaves residual carbon with gaps that potentially form new

micropores. Increasing the number of pores will have a direct impact on increasing the pore volume of the activated carbon [5].

The PGNS does not have a better surface area compared with the CNT composite. It is suspected that this is due to the PGNS being directly exposed to residual oxygen in the carbonization and activation processes inside the furnace, resulting in a gasification process as a continuation of the pyrolisis process that causes most of the carbon to be converted into CO_2 and H_2O [6].

The oxidation process causes damage to the pore walls of the carbon (collapse), which leads to a reduction of the surface area. Collapse of the pore wall is evidenced by an average pore size for PGNS that is lower than that of CNT composite. Damage to the pore wall causes burst pores to become smaller [7].

3.2 Surface Characteristics

Surface area testing was done using the N_2 adsorption-desorption method to obtain how the layers, volume, and pores of the coconut shell substrate were formed, as can be seen in Figures 3, 4, and 5.

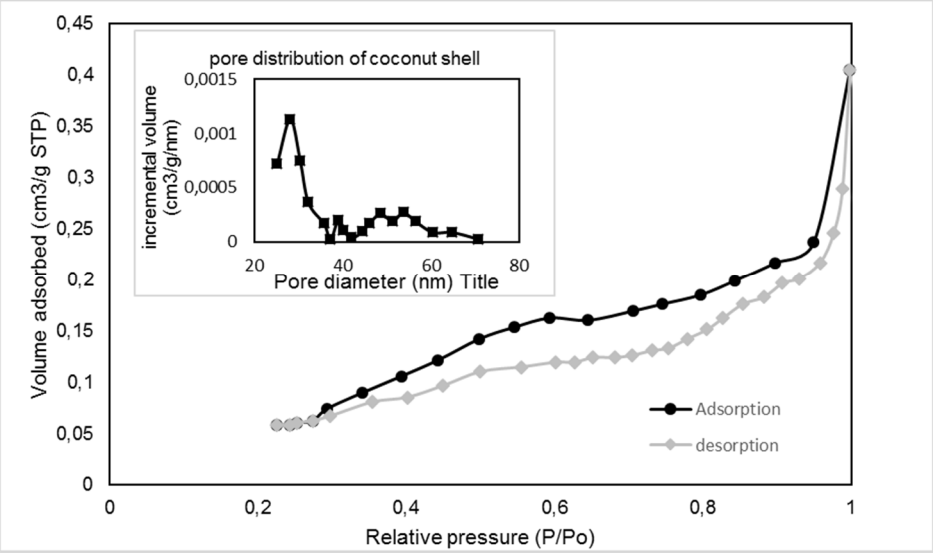

Figure 3 Adsorption desorption isotherm curve and pore size distribution of coconut shell.

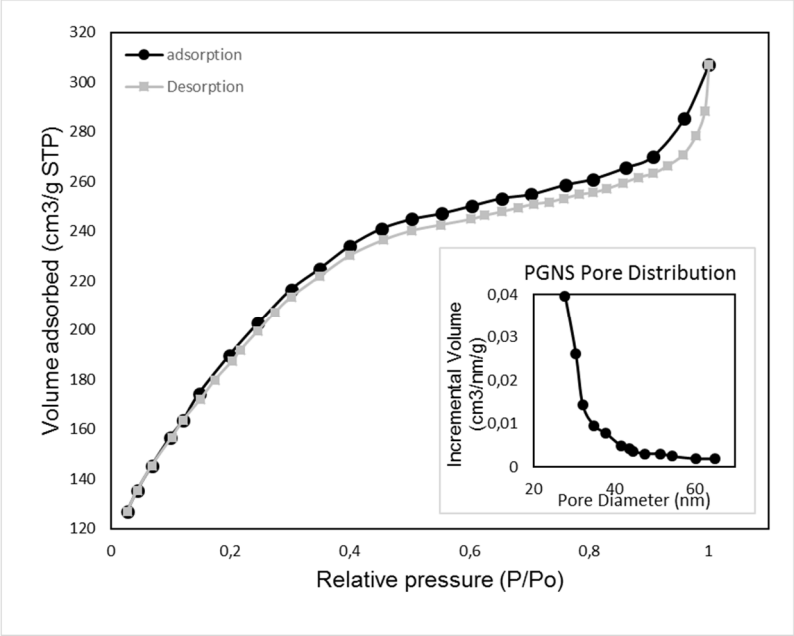

Figure 4 Adsorption desorption isotherm curve and pore size distribution of PGNS.

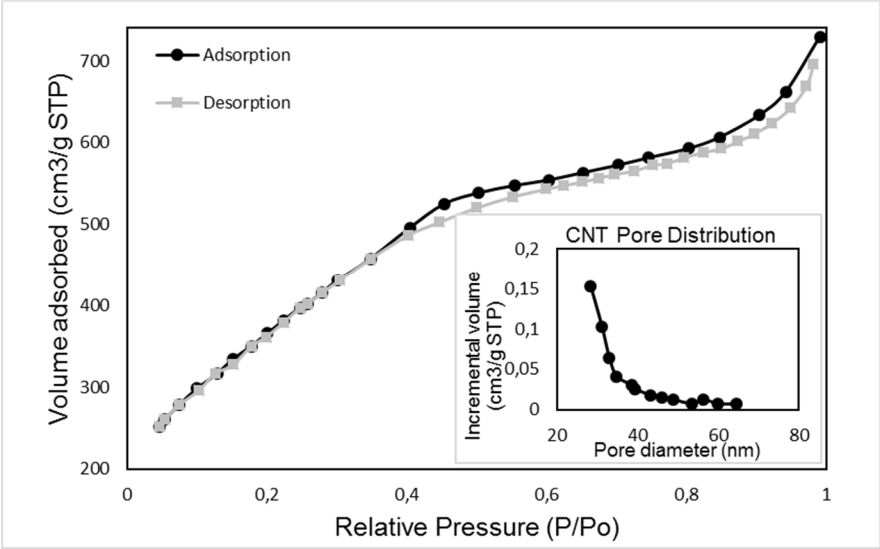

Figure 5 Adsorption desorption isotherm curve and pore size distribution of CNT.

Based on Figures 4 and 5, it can be stated qualitatively that the two types of activated carbon modification follow type IV of the isotherm curve based on the IUPAC classification system, as is shown by the hysteresis loop in the curve. This indicates the formation of multilayer adsorption with a solid mesopore structure [8]. The presence of significant nitrogen absorption at a pressure from 0.0 to 0.4 marks that there are micropores on part of the activated carbon surface [9]. When compared with Figure 3, it can be stated qualitatively that carbonization and activation do not damage the basic structure of the carbon compounds in the lignocellulose of the coconut shell. On the other hand, it has been proven that carbonization and activation can increase the pore volume of activated carbon either in PGNS or CNT. In addition, the pore distribution after carbonization and activation decreases from 8-10 nm to 3-8 nm. A substantial reduction in the amount of mesopores is caused by loss or destruction of the walls of the activated carbon [7]. The high specific surface area and the amount of mesopores provide a convenient adsorption of ions, which diffuse into the surface of the electrode [9].

The combination of activator and temperature plays an important role in terms of forming the activated carbon structure. The surface morphologies of the PGNS and the CNT composite can be seen in Figure 6.

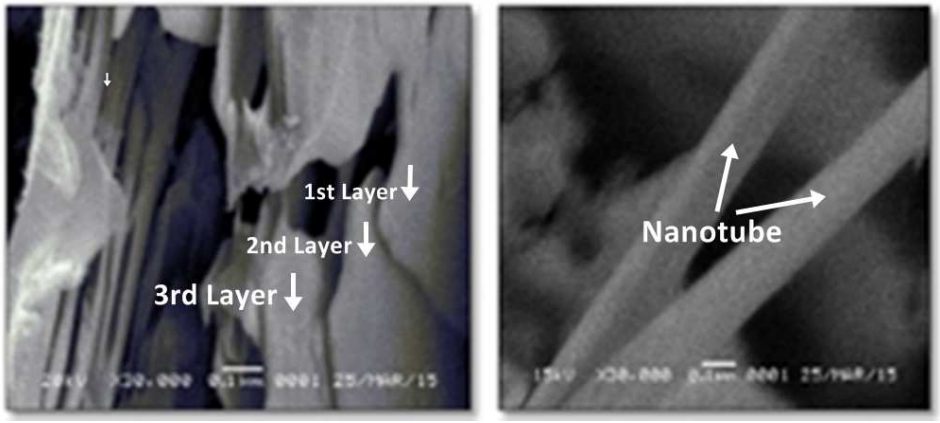

(a) (b)

Figure 6 Morphology activated carbon: (a) PGNS and (b) CNT composite.

Figure 6 shows that there was no microstructure either in the PGNS or the CNT composite. In Figure 6(a) layer stacks can be seen that are suspected to be the piles of the graphite sheet, identical to commercial graphene by S-Nano (2011) with a surface area not far from 500 m^2/g. The $FeCl_3$ served as catalyst forming PGNS, where the $FeCl_3$ substrate reacted with the carbon to form intermediate

Fe_3C layers at a temperature of 700 °C. Along with increasing temperature, the carbon atoms diffused out and apart from each other, forming a 2D layer of carbon atoms [9]. The Fe_3C that forms during the synthesis of PGNS can act as a template to limit the carbon graphitization along the 2D plane, like planar Ni and Cu substrates for preparing graphene by CVD methods [9].

In Figure 6(b) it can be seen that there are sharp CNTs with a diameter of 150-175 nm. The results are identical to those from the study conducted by Mopoung [11], however, the number of formed CNTs was higher in the present study. This is presumably because of the separate stages of nanotube formation conducted after the carbonization and activation stages were carried out at lower temperatures. The precursor carbonization and activation stages yielded activated carbon with a solid graphite structure separated from the non-carbon compounds [5]. Meanwhile, during the stage of carbonization, the activation and formation of CNTs in this research was done in one step, so there is a high probability of side reactions that inhibit the decomposition of the carbon on the catalyst substrate, Ni and Fe, form its carbide compounds, Ni_3C and Fe_3C. Ni_3C and Fe_3C are intermediate products of the CNT constituents [10].

According Ruskov, *et al.*, Fe_3C is mainly found at the interface of the CNT and the substrate as observed with Mössbauer spectroscopy analysis [11]. The existence of nickel in stainless steel is expected to form Ni_3C, which could act as a catalyst in the CNT composite. Nevertheless, the amount of Ni_3C formation in this experiment could not be shown by XRD [12]. The details can be seen in Figure 7.

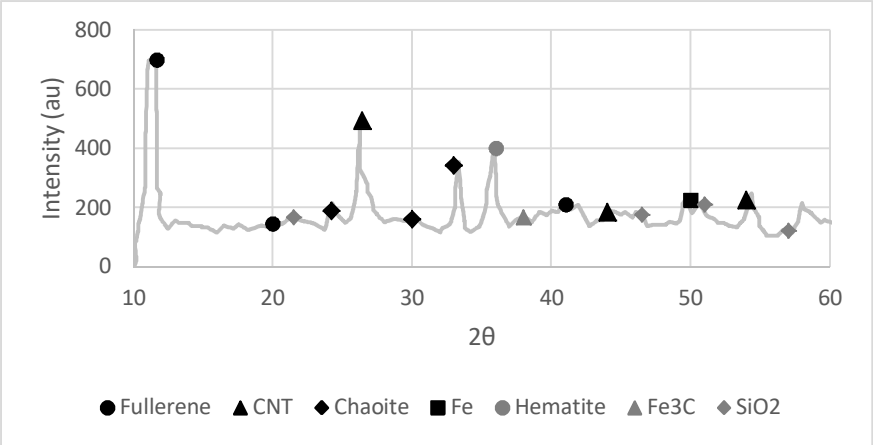

Figure 7 XRD patterns of CNT composite.

Figure 7 shows that the content of the formed activated carbon was quite varied. Apart from CNT at angles of 2Θ 26, 44, and 54°, also carbon fullerene (11, 20, and 41.4°) and chaoite (24.5, 30, and 34°) were observed. In addition, this test indicated that the product still had impurities, such as iron (49°), hematite (36° and 58°), Fe_3C (28°), and SiO_2 (21.5, 46, 51.5, and 56.5°). The presence of impurities is caused by α-Fe derived from the activator $FeCl_3$ by dissociation and reaction with most of the carbon and oxygen still contained in the tube and α-Fe also originating from Fe that was in the tube itself [13]. Supposedly, the α-Fe, Fe_3C, and $FeCl_3$ was dissolved by washing with HCl. However, the use of HCl with a concentration of 0.5 M did not dissolve all the impurities. In a similar study, conducted by Sun *et al.* in 2012, with the use of an HCl 2M solution the impurities were completely dissolved. The SiO_2 impurities probably derived from the ash that had already been formed from the coconut shell substrate.

In this study, the average crystal size of the carbon particles measured by XRD was calculated using the following Scherrer equation,

$$L = \frac{K\lambda}{B\cos\Theta} \quad (1)$$

Based on Eq. (1), the average size of the crystals was determined by selecting the three highest peak diffraction angles of the activated carbon with a wavelength of 1.54 nm copper anode source. The results are shown in Table 3.

Table 3 Crystal size of activated carbon.

2Θ	FWHM	Θ(degree)	Θ(radian)	Cos Θ	L (nm)
11.3	0.601	5.65	0.098651	0.995138	2.32
26.26	0.655	13.13	0.229254	0.973836	2.17
33.28	0.565	16.64	0.29054	0.958089	2.56

Based on Table 3, the average crystal size was 2-3 nm. The crystal size resulted in a pore diameter that was not much different from that from the BET analysis: 2.8-3.2 nm. SEM and XRD testing was not able to determine the type of formed CNT. However, based on the diameter (150-175 nm) and the size of the crystals, the formed CNT is considered multi-walled nanotubes (MWNT). Mopoung [13] synthesized CNT through a CVD process and the result was MWNT type CNT with diameter 119-192 nm.

3.3 Effect of CNT Composite Addition to PGNS

Determination of the effect of CNT composite addition to PGNS on the performance of the activated carbon as the supercapacitor electrode can be seen through cyclic voltammetry testing. This test was aimed at calculating the capacitance of the cells. Two electrodes with a size of 1 x 1 cm^2 were used in

the test. The activated carbon was put on top of a stainless steel mesh current collector and the NiO pair on top of a carbon cloth current collector, while the two electrodes were separated by a Nafion 212 separator, as shown in Figure 8.

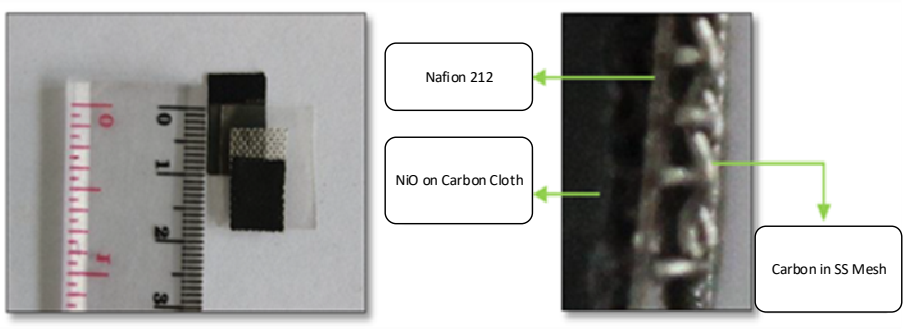

Figure 8 Supercapacitor cell structure.

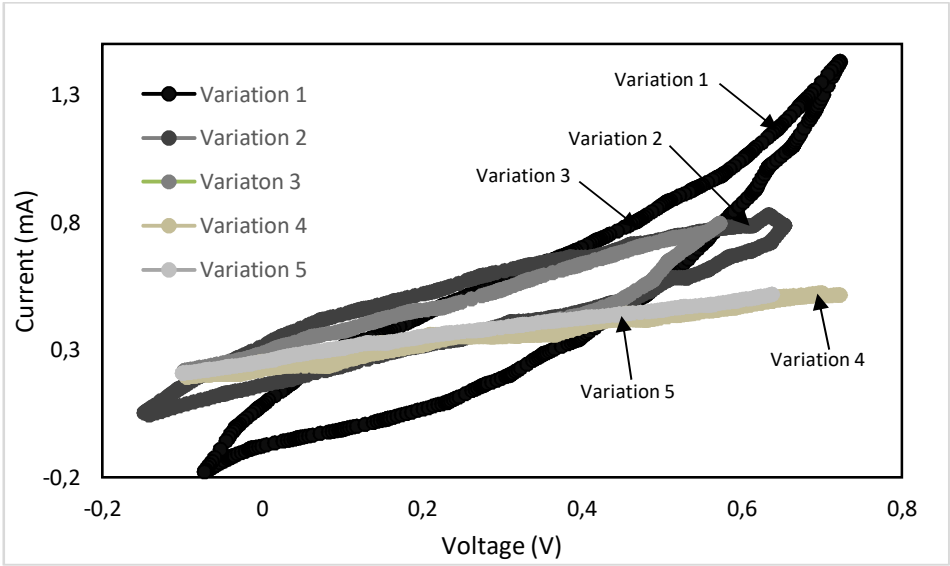

Figure 9 Voltammogram for composition to capacitance effect.

In Figure 9 we can see that with the addition of the CNT composite, the width of the distance between the charging and discharging curve increased. This indicates that electrolyte diffusion and electrode interphase barriers became smaller [14]. The ease of the ions to pass through the channel pores of the activated carbon and the double layer created on the electrode and electrolyte interphase may increase the amount of electric charge that can be stored in the cells. The fourth composition variation showed that there is an instability curve

that only occurs at a relatively high voltage of 0.4-0.7 V. It is presumed that the difficulty of electrons moving at a relatively high voltage is due to the splicing system at the time of testing.

Increasing the amount of electric charges that can be stored will increase cell capacitance. Good conductivity of CNT also plays a role in increasing capacitance [15]. The generated capacitance for each variation is shown in Table 4.

Table 4 Capacitance of each composition of activated carbon.

Composition	Concentration G (%)	Concentration CNT (%)	Capacitance (F/g)
1	100	0	1.43
2	90	10	1.60
3	80	20	2.79
4	70	30	3.69
5	60	40	5.69

Based on Table 4, along with the addition of CNT composite to every variation, the capacitance generated also increased. This is in accordance with the study conducted by Khomenko, *et al.* [15], in which the addition of 30% commercial CNT MnO2 electrode increased the capacitance from 0.1 to 138 F/g.

3.4 The Effect of Scan Rate to Cell Capacitance

This research tested cell stability based on variations of scan rate in order to determine the stability of CNT composite as additive in supercapacitor cells.

Based on Figure 10, the higher scan rates have a more elongated cycle than the lower scan rates. This is an indication of the existence of barriers for the ion transfer from the electrolyte to get to the electrode surface, so not all the activated carbon pores can be accessed [14]. The charging-discharging process should take place quickly, but the presence of pseudocapacitance derived from the NiO electrochemical reaction causes the discharge to take longer. In addition, when the scan rate is high, the ions collide very fast but tend to be irregular in reaching the electrode-electrolyte boundary layer, so the double layer formed is not perfect and can reduce the capacitance. The tendency of the cycle to form a sloped curve indicates that there was a leak current or a side reaction between the electrolytes and functional groups on the activated carbon. If the sealing system is still open without vacuum enabled, then the oxygen functional group becomes reactive and unstable, which disrupts the ion transfer [16].

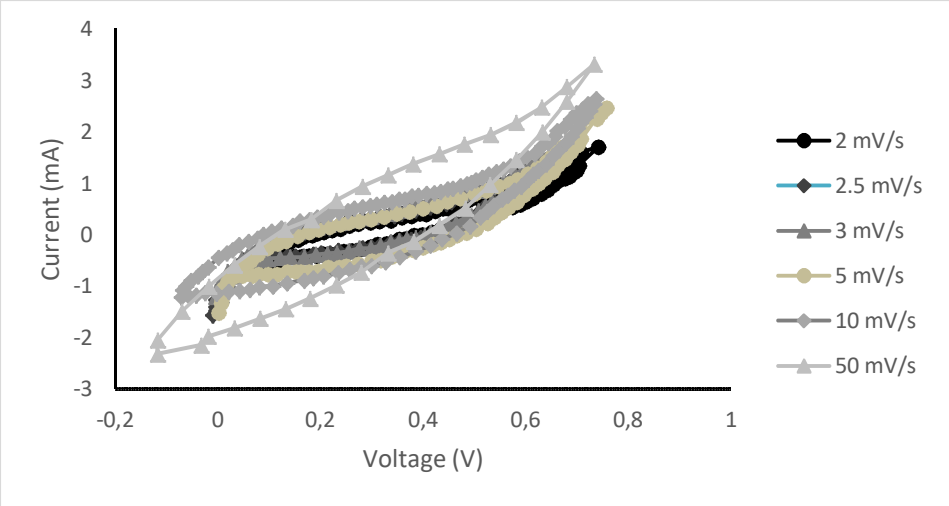

Figure 10 Voltammogram curves at various scan rates.

3.5 Cell Impedance

Cell impedance testing was conducted to compare the natural resistance characteristic to the supercapacitor resistance characteristic. The observations are depicted as a Nyquist curve in Figure 11 and Table 5. The resistance was obtained from modeling or fitting the equivalent circuit in Figure 12.

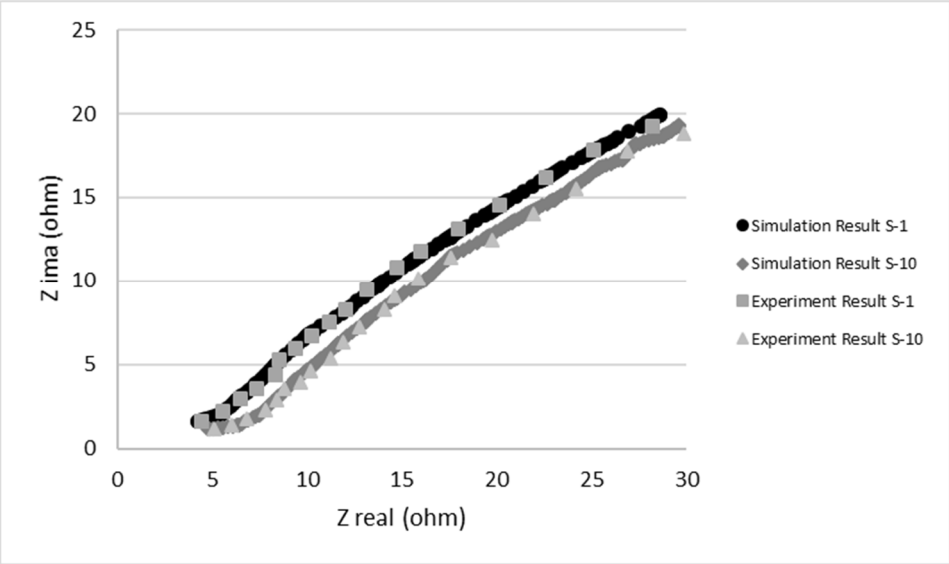

Figure 11 Cell impedance.

Table 5 Cell impedance.

Cycle	Parameter	
	Rs (Ω)	Rp (Ω)
1	4.7	5.05
10	4.9	5.4

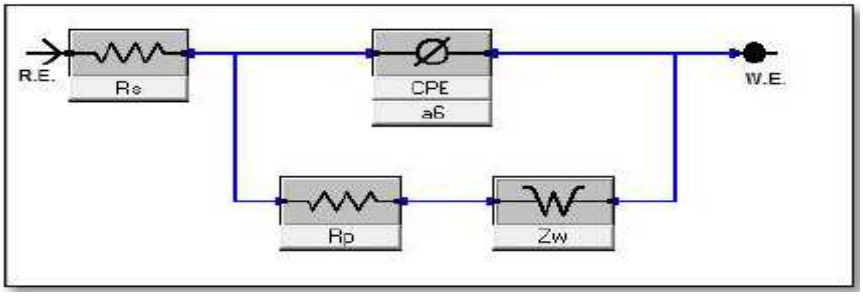

Figure 12 EIS Randles circuit.

At the beginning of the cycle at a high frequency, there was ohmic resistance (Rs), which indicates a charge barrier on the electrode surface. After the 10^{th} cycle, the resistance was increased and the curve shifted slightly to the right. This may indicate a contact resistance at the electrode and the current collector. Furthermore, the frequency indicates electrolyte interphase resistance (Rp) creating a domino effect in the electrode pores.

At the beginning of the semi-circle cycle, interphase resistance was invisible. However, along with the increase to the 10^{th} cycle, the resistance started to increase, marked by the distance between the real impedance and the ordinate axis getting wider. The difficulty the ions have of getting into the pores can inhibit the formation of the double layer. The reaction that forms pseudocapacitance tends to be slower in releasing ions also supports a decreasing capacitance. The electrochemical reaction of pseudocapacitance formation is shown in Eq. (2).

$$NiO + OH^- \leftrightarrow NiOOH + e^- \quad (2)$$

Compared with another studies, the resistance of the cells in this study was higher. Several factors could explain this phenomenon. It is assumed that the connection between current collector, electrode and electrolyte was not optimal. In addition, the opening cells without good sealing system also accelerated the drying of the electrolyte so that the ions had difficulty to diffuse in the charging-discharging process. A comparison of the resistance in various studies is shown in Table 6.

Table 6 Comparison of resistance in various studies.

Researcher	Parameter	
	Rs (Ω)	Rp (Ω)
Sun *et al.*, 2013	0.14	0.56
Basri *et al.*, 2013	0.41	0.49
Deraman *et al.*, 2013	0.39	0.54
This study	**4.9**	**5.4**

3.6 Cycle Stability

The repeated use of a supercapacitor requires good stability from its materials. The effect of the number of cycles on cell stability is shown in Figure 13. Figure 13 shows a symmetrical triangle curve. This indicates good cell stability, especially during discharge because there is no voltage drop at this stage [17]. Until the 10th charge-discharge cycle, the curve is likely to be stable. This also indicates that the cell resistance did not increase drastically.

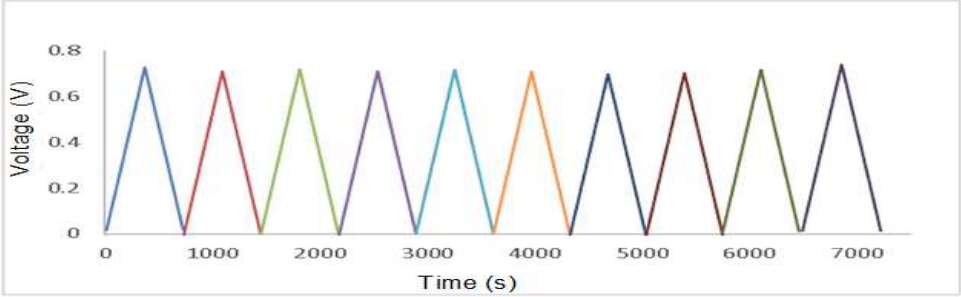

Figure 13 Charge-discharge cell stability.

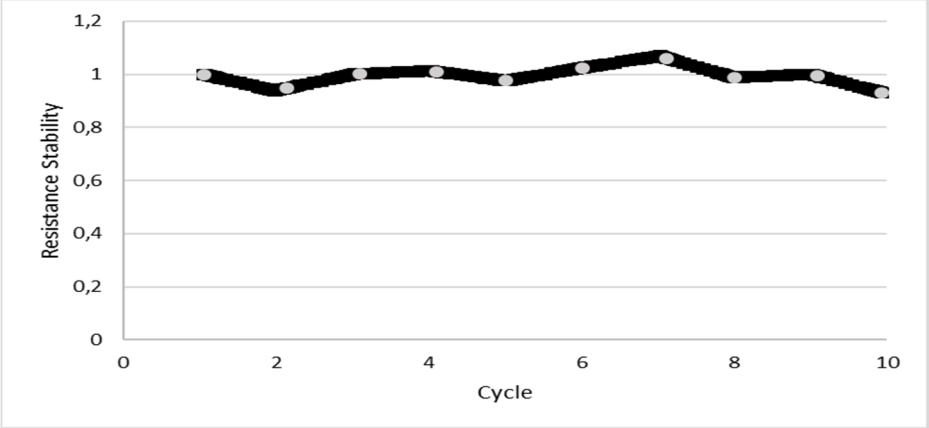

Figure 14 Stability curve of capacitance for every cycle.

The stability curve can also be interpreted as in Figure 14. Based on Figure 14, the supercapacitor cell durability was relatively good and stable throughout the testing cycle.

Fluctuation in capacitance exceeding 100% in stability is suspected, caused by an irreversible reaction between the electrolyte and hydroxyl group in the electrode boundary, which would increase the charge release in the next cycle. This phenomenon occurs regularly [16]; the reaction is shown in the Eqs. 3 and 4.

$$NiO + H_2O \rightarrow Ni(OH)_2 \quad (3)$$

$$Ni(OH)_2 + OH^- \leftrightarrow NiOOH + H_2O + e^- \quad (4)$$

The capacitance of the supercapacitor tended to be stable and by seeing fluctuations and mechanism that may occur, the cell supercapacitor in this study can be expected to be used longer. The durability of the cell supercapacitor in this study reached 94.1% after 10 cycles.

4 Conclusion

Modified activated carbon from PGNS and CNT composite was successfully produced by simultaneous carbonization and activation. However, the simultaneous processes caused many impurities, so not all the structures of PGNS and CNT composite were formed. Increasing the CNT composite's concentration increased the capacitance of the supercapacitor cells. However, the capacitance decreased along with the increase of the scan rate. At the 10^{th} charge-discharge cycle at a constant scan rate, the supercapacitor cells showed good stability.

Acknowledgements

The research described in this paper was fully supported by the Process Safety and Corrosion Control Laboratory, Department of Chemical Engineering, Institut Teknologi Bandung, Indonesia.

Nomenclature

Θ	=	Bragg angle (^{o})
L	=	Average crystal size (nm)
K	=	Scherrer constant of 0.94
Λ	=	Wave length (nm)
B	=	Width of half maximum peak diffraction result (radian)

References

[1] Bansal, R. C. & Goyal, M., *Activated Carbon Adsorption*, Boca Raton, CRC Press, 2005.

[2] Basu, P., *Biomass Gasification and Pyrolisis: Practical Design and Theory*, 2nd ed., Oxford, Elsevier, 2010.

[3] Anonym, Dewan Kelapa Indonesia, http://www.dekindo.com/acara/seminar.php (14 July 2014).

[4] U.S. Energy Information Administration, *Annual Energy Outlook 2014*, 2014.

[5] Gu, W., Peters, N. & Yushin, G., *Functionalized Carbon Onions, Detonation Nanodiamond and Mesoporous Carbon As Cathodes in Li-Ion Electrochemical Energy Storage Devices*, Carbon, **53**, pp. 292-301, 2013.

[6] Halper, M.S., & Ellenbogen, J.C, *Supercapacitors: A Brief Overview*. MITRE Corporation, https://www.mitre.org/, 2006.

[7] Jain, A. & Tripathi, S.K., *Fabrication and Characterization of Energy Storing Supercapacitor Devices Using Coconut Shell Based Activated Charcoal Electrode*, Materials Science and Engineering B: Solid-State Materials for Advanced Technology, **183**(1), pp. 54-60, 2014.

[8] Jaramillo, J.P., Álvarez, M. & Gómez, V., *Oxidation of Activated Carbon by Dry and Wet Methods: Surface Chemistry and Textural Modifications*, Fuel Processing Technology, **91**, pp. 1768-1775, 2010.

[9] Khomenko, V., Pinero, R.E. & Beguin, F., *Hybrid Supercapacitors Based on a MnO_2/Carbon Nanotubes Composites*, New Carbon Based Materials for Electrochemical and Fuel Cells Energy Storage Systems: Batteries, Supercapacitors, pp. 33-40, 2005.

[10] Marsh, H. & Rodriguez, F., *Activated Carbon*, Elsevier Science & Technology Books, 2006

[11] Mopoung, S., *Occurrence of Carbon Nanotube from Banana Peel Activated Carbon Mixed with Mineral Oil*, International Journal of the Physical Science, **6**(7), pp. 1789-1792, 2011.

[12] Sun, L., Tian, C., Li, M., Meng, X., Wang, L., Wang, R., Yin, J. & Fu, H., *From Coconut Shell to Porous Graphene-like Nanosheets for High Power Supercapacitors*, Journal of Materials Chemistry A, **1**(21), pp. 6462-6470, 2013.

[13] Yu, A., Chabot, V. & Zhang, J., *Electrochemical Supercapacitors for Energy Storage and Delivery*, Boca Raton, CRC Press, 2013.

[14] Zheng, C., Qian, W., Cui, C. & Xu, G., *Carbon Nanotubes for Supercapacitors: Consideration of Cost and Chemical Vapor Deposition Techniques*, Journal of Natural Gas Chemistry, **21**(3), pp. 233-240, 2012.

[15] Kalyani, P., Anitha, A. & Darchen, A., *Activated Carbon from Grass – A Green Alternative Catalyst Support for Water Electrolysis*, International Journal of Hydrogen Energy, **38**(25), pp. 10364–10372, 2013.

[16] Ruskov, T., Spirov, L., Ritschel, M., Muller, C., Leonhardt, A. & Ruskov, R., *Mossbauer Morphological Analysis of Fe-filled Multiwalled Carbon Nanotube Samples*, Journal of Applied Physics, **100**, pp. 084326-084328, 2006.

[17] Weissker, U., Hampel, S., Leonhardt, A. & Buchner, B., *Carbon Nanotubes Filled with Ferromagnetic Material,* Journal of Material, **3**(8), pp. 4387-4427, 2010.

[18] Borjesson, A. & Kim, B., *First Principles Studies of the Effect of Nickel Carbide Catalyst Composition on Carbon Nanotube Growth,* Journal of Physical Chemistry*,* **114**(42), pp. 18045-18050, 2010.